Supplementary material: the spatial structure of antagonistic species affects coevolution in predictable ways

Jean P. Gibert[1,*], Mathias M. Pires[2], John N. Thompson[3] and Paulo R. Guimarães Jr.[2]

[1] Laboratorio de Paleobiología, Sección Paleontología, Facultad de Ciencias de la Universidad de la República, Iguá 4225, Montevideo 11400, Uruguay.

[2] Departamento de Ecologia, Instituto de Biociências, CP 11294, Universidade de São Paulo, São Paulo 05422-970, Brazil.

[3] Department of Ecology and Evolutionary Biology, University of California - Santa Cruz, Santa Cruz, California 95064, USA.

*Current address: School of Biological Sciences, University of Nebraska – Lincoln, 410 Manter Hall, Lincoln, Nebraska 68588-0118, USA.

CONTENTS

A) Matching Alleles Model: single-site, two-sites and n-site dynamics.

The Matching Alleles Model is a simple model in discrete time that assesses species coevolution within a given site (Seger 1988, Gavrilets and Hastings 1998). During the last decade it has been successfully used to explore species coevolution in space-structured populations (e.g. Nuismer *et al.* 1999, Gomulkiewicz *et al.* 2000, Gomulkiewicz *et al.* 2003). Both the model and its assumptions are explained in detail in the Methods section. Here we will focus on showing analytically its behavior in a single site model, its numerical behavior in a two-site case as well as an analytical proof for it in a special case and we will finally extend it to a star subgraph with *n*-sites in which coldspots are at equilibrium.

i) Single-site case: local stability of polymorphic equilibrium

Let us consider the case in which two species coevolve through reciprocal antagonistic interactions in a single site and each species has two alleles, namely: X and x for the parasite (or predator) and Y and y for the host (or prey). Let us define X_t, Y_t, x_t and y_t as the allele frequencies at time t of alleles X, Y, x and y respectively, such that $x_t = 1 - X_t$ and $y_t = 1 - Y_t$. Following Seger 1988, the fitness equations associated to this system are:

$$\begin{cases} W_{Xt} = 1 + \alpha Y_t \\ W_{xt} = 1 + \alpha(1 - Y_t) \\ W_{Yt} = 1 - \alpha X_t \\ W_{yt} = 1 - \alpha(1 - X_t) \end{cases}, \qquad (1)$$

where α is the fitness sensitivity on species interactions. Then, allele frequencies at time $t+1$ are defined as:

$$\begin{cases} X_{t+1} = \dfrac{X_t W_{Xt}}{X_t W_{Xt} + (1 - X_t) W_{xt}} \\ Y_{t+1} = \dfrac{Y_t W_{Yt}}{Y_t W_{Yt} + (1 - Y_t) W_{yt}} \end{cases}. \qquad (2)$$

At equilibrium, $\Delta X = X_{t+1} - X_t = 0$ and $\Delta Y = Y_{t+1} - Y_t = 0$. Solving $\Delta X = 0$ and $\Delta Y = 0$ for X_t and Y_t gives us the equilibrium allelic frequencies (let us name them X^* and Y^*):

$$\begin{cases} X^* = 0, & Y^* = 0 \\ X^* = 0, & Y^* = 1 \\ X^* = \frac{1}{2}, & Y^* = \frac{1}{2} \\ X^* = 1, & Y^* = 0 \\ X^* = 1, & Y^* = 1 \end{cases} . \tag{3}$$

It can be seen that there is one single polymorphic equilibrium, $X^* = 1/2$ and $Y^* = 1/2$. In all other equilibria populations are monomorphic due to the loss of one allele in each species.

We assessed whether the polymorphic equilibrium is locally stable by studying the Jacobian matrix of the system, evaluated at $X^* = 1/2$ and $Y^* = 1/2$:

$$J\big|_{X^*, Y^* = \frac{1}{2}} = \begin{pmatrix} 1 & \frac{\alpha}{2+\alpha} \\ -\frac{\alpha}{2-\alpha} & 1 \end{pmatrix} . \tag{4}$$

The eigenvalues of such matrix tell us whether the system returns to equilibrium or goes away from it after a small perturbation. Indeed, if the absolute value of the real part of the eigenvalues of the Jacobian is smaller than one, the equilibrium is stable. If the absolute value of the real part of the eigenvalues of the Jacobian is bigger than one, then the equilibrium is unstable. For (4), we get the following eigenvalues:

$$\lambda_1 = 1 + \frac{\alpha\sqrt{(\alpha^2 - 4)}}{(\alpha^2 - 4)} \tag{5}$$

$$\lambda_2 = 1 - \frac{\alpha\sqrt{(\alpha^2 - 4)}}{(\alpha^2 - 4)} . \tag{6}$$

In our case, α is always positive. For $\alpha > 0$ ($\alpha \neq 2$) there is at least one eigenvalue with absolute value larger than one. Therefore, the single-site MAM has a single polymorphic

equilibrium that is unstable. If $0 < \alpha < 2$, then $(\alpha^2 - 4) < 0$ and the eigenvalues will have an imaginary part, implying that a small perturbation will carry allelic frequencies away from $X^* = Y^* = 1/2$ in the form of increasing oscillations. If $\alpha > 2$, the eigenvalues are purely real and a small perturbation will lead to a monotonic increase (decrease) in allelic frequency until a fixation (elimination) point is reached. For $\alpha = 2$, the eigenvalues are not defined and local stability analysis is uninformative.

ii) Two-site case: qualitative behavior

Here we reviewed the results by Nuismer *et al.* 1999 in the two-site case. Let us consider two sites connected by migration of individuals of two coevolving species. One of the sites is a coevolutionary hotspot and the other one is a coevolutionary coldspot. Thus, the structure of selection imposed by the interaction varies among sites. In the coevolutionary hotspot the antagonistic interaction between species leads to reciprocal selection. In the coldspot, selection is non-reciprocal and there is a fitness gain for one of the interacting species, whereas the interaction has no effect in the fitness of the other species. As found in previous studies (Nuismer *et al.* 1999), the coevolutionary dynamics within the hotspot are deeply influenced by gene flow. When there is no gene flow between sites, hotspot allelic frequencies oscillate unstably (fig. A-1) but when there is gene flow, hotspot allelic frequencies oscillate stably (fig. A-2). That is, gene flow among sites allows polymorphism maintenance in hotspots. When there is gene flow, coevolutionary oscillations are dampened, leading the population to a stable polymorphic state (fig. A-2) and therefore dynamics differ between one-site and two-sites MAMs.

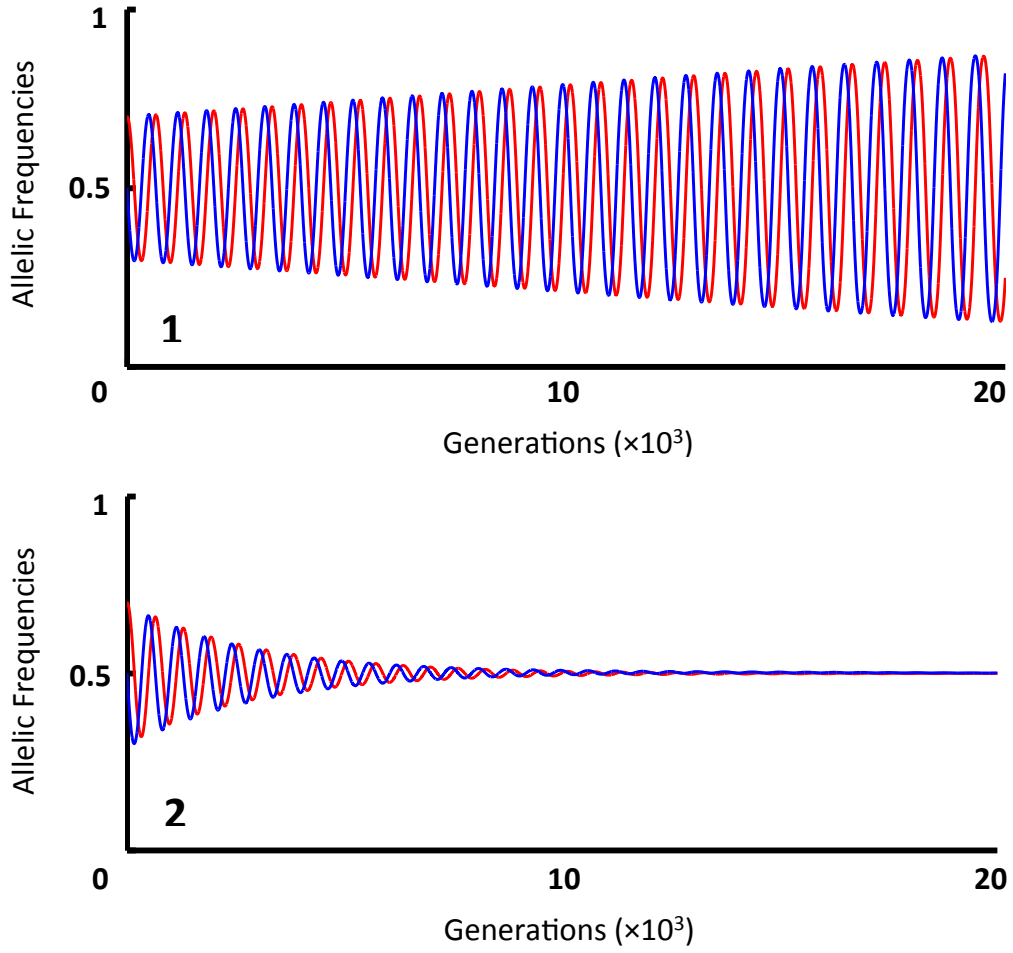

Figure A: Coevolutionary dynamics for a two-site Matching Alleles Model with two coevolving species. Red curve describes the change in one of the alleles of the parasitic species while the blue curve tracks the change in one of the alleles of the host species within the hotspot. **(1)** No gene flow scenario ($\sigma^2 = 0; \alpha = 0.02$) and **(2)** scenario with gene flow connecting the hotspot and the coldspot ($\sigma^2 = 0.23; \alpha = 0.02$).

iii) Two-site case: local stability

Let us now consider the same two-sites system in which there is a coevolutionary hotspot connected to a coevolutionary coldspot. We restrict our analysis to the special case in which the coevolutionary coldspot is at equilibrium, and gene flow is unidirectional, only

happening from coldspots to hotspots. In that case, only hotspot dynamics will be affected by gene flow. Following our Methods section, species in the hotspot interact, reproduce and then individuals from the coldspot arrive.

Hotspot fitness functions can be described using equations (1) of the online appendix. There is no need to consider coldspot fitness functions as the coldspot is assumed not to receive migrants from the hotspot and to be at equilibrium. Again, the MAM will have one single polymorphic equilibrium at $X^* = Y^* = 1/2$, and four monomorphic equilibria. The reproduction step is embodied by equations (2) of the online appendix and migration was described in the main text by equation (7). Here we will consider a special case of such equation, by assuming that gene flow is constant; let us call μ the level of gene flow. This modified equation yields post-migration frequencies (X'_{t+1}, Y'_{t+1}), described by the following expression for the two sites case:

$$\begin{cases} X'_{t+1} = (1-\mu)X_{t+1} + \mu C \\ Y'_{t+1} = (1-\mu)Y_{t+1} + \mu C \end{cases}, \qquad (7)$$

where C represents the allelic frequency of interest in the coldspot. Since coldspots are at equilibrium, $C = 1/2$.

Now we can find the equilibrium values by solving $\Delta X = \Delta Y = 0$ as in the single-site case. Five equilibria can be found that way, one of which is $X^* = Y^* = 1/2$, the only polymorphic equilibrium. Let us assess the stability of the polymorphic equilibrium, applying the technique used for the single-site case. By doing so, the Jacobian of the system evaluated at $X^* = Y^* = 1/2$ is:

$$J\big|_{X^*, Y^* = \frac{1}{2}} = \begin{pmatrix} 1-\mu & \dfrac{\alpha(1-\mu)}{2+\alpha} \\ -\dfrac{\alpha(1-\mu)}{2-\alpha} & 1-\mu \end{pmatrix}. \qquad (8)$$

It is worth noticing that when $\mu = 0$, the Jacobian of this special two-sites system is reduced to the Jacobian of the single-site case. The eigenvalues of (8) are:

$$\lambda_1 = (1-\mu) + \frac{\alpha\sqrt{(\mu-1)^2}}{\alpha^2 - 4} \tag{9}$$

$$\lambda_1 = (1-\mu) - \frac{\alpha\sqrt{(\mu-1)^2}}{\alpha^2 - 4} \tag{10}$$

If $\mu < 1$ the eigenvalues are complex and the system will undergo either stable or unstable oscillations. For the system to be stable, the fitness sensitivity must be $0 < \alpha < 1$, with bounded levels of gene flow, namely $1 - \sqrt{1-\alpha^2} < \mu < 1 + \sqrt{1-\alpha^2}$. In other words, gene flow needs to be sufficiently high compared to the fitness sensitivity due to reciprocal selection in order to yield a polymorphic equilibrium, but not too high or such polymorphic equilibrium would be unstable.

iv) Extension to n-sites

The special case for two-sites described in the previous section can be extended to n-sites, with the same assumptions. In such case, the hotspot would receive migrants from $n-1$ coldspots, but coldspots would receive none from the hotspot. Coldspots are also at equilibrium. Here, the spatial structure of the *n*-sites set of populations can be considered star-shaped, as a single hotspot receives migrants from $n-1$ adjacent coldspots. In the two-sites case, the level of gene flow, μ, was such that adding the levels of gene flow across all sites is equal to one. Then two sites A and B have gene flow levels μ and $1-\mu$, such that $\mu + (1-\mu) = 1$, and three sites A, B and C will have migration levels $\mu/2$, $\mu/2$ and $1-\mu$ respectively, which ensures that $\mu/2 + \mu/2 + (1-\mu) = 1$. If we continue adding sites, then *n* connected sites $A_1, \ldots, A_n$ will have migration levels $\mu/(1-n)$, $\mu/(1-n)$, … , $1-\mu$

respectively, which also adds up to one. In this case, hotspot's post-migration frequencies become:

$$\begin{cases} X'_{t+1} = (1-\mu)X_{t+1} + \sum_{i=1}^{n-1} \frac{\mu}{n-1} C \\ Y'_{t+1} = (1-\mu)Y_{t+1} + \sum_{i=1}^{n-1} \frac{\mu}{n-1} C \end{cases}, \tag{11}$$

where C is the coldspot equilibrium frequency, namely $1/2$. Then, (11) can be rearranged into:

$$\begin{cases} X'_{t+1} = (1-\mu)X_{t+1} + (n-1)\frac{\mu}{n-1} C \\ Y'_{t+1} = (1-\mu)Y_{t+1} + (n-1)\frac{\mu}{n-1} C \end{cases}, \tag{12}$$

which is equal to (7) after simplification. Hence, n-site dynamics are undistinguishable from two-site dynamics in this special case. In other words, the chance of maintaining polymorphisms is the same for the n-sites case and for the two-sites case.

We have therefore shown that the stability of two-site and *n*-site models in the case where coldspots are at equilibrium and gene flow is unidirectional can be mathematically equivalent. These results show that the spatial structure of interacting populations does not always influence coevolutionary outcomes under these very restrictive assumptions. Nevertheless, these results just hold for the very simple spatial structure considered, and uncovers the need for incorporating more complex and realistic spatial structures while relaxing the above assumptions. Unfortunately, this task would be prohibitive to undertake analytically. In the main text we show how relaxing the unrealistic assumptions of unidirectional gene flow and coldspots at equilibrium while taking into account more realistic spatial structures such as structures that have different coldspot spatial configurations and hotspot location yield significantly different results.

B) Laplacian matrix of spatial subgraphs

i) The Laplacian matrix

In this section we introduce the Laplacian matrices, which allowed us to assess the potential of a given spatial subgraph to exhibit spatial variation in coevolutionary dynamics (see Methods). For any given simple graph with *n* nodes, we can define two associated matrices: the adjacency matrix, and the degree matrix. The adjacency matrix is $\mathbf{A} = [\alpha_{ij}]_{n\times n}$ where:

$$\alpha_{ij} = \begin{cases} 1, & \textit{if nodes i and j are connected} \\ 0, & \textit{otherwise} \end{cases} . \quad (13)$$

The associated *degree* matrix is $\mathbf{D} = [d_{ij}]_{n\times n}$. The degree matrix is diagonal, with the number of links of each node *i*, or degree (k_i). Formally:

$$d_{ij} = \begin{cases} k_i & i = j \\ 0\,, & i \neq j \end{cases} , \quad (14)$$

The *Laplacian* matrix is $L = [l_{ij}]_{n\times n}$, such that $L = \mathbf{D} - \mathbf{A}$. Hence:

$$l_{ij} = \begin{cases} k_i\,, & \textit{if } i = j \\ -1\,, & \textit{if } i \neq j \textit{ and nodes i and j are connected} \\ 0\,, & \textit{otherwise} \end{cases} . \quad (15)$$

The *Laplacian* matrix can be used to investigate graph connectivity (Mohar 1997) and how prone a system is to exhibit synchronized dynamics (Barahona and Pecora 2002, see "*Synchronizability and the Laplacian matrix*" section). Also note that $\sum_j l_{ij} = k_i - \sum_{j\neq i} \alpha_{ij} = k_i - k_i = 0$ in any graph without loops (i.e. a graph where $\alpha_{ii} = 0$), which ensures that at least one eigenvalue is zero, and that all others are real and can be ordered as $0 = \lambda_1 < \lambda_2 < \ldots < \lambda_{\max}$.

ii) Synchronizability and the Laplacian matrix

In this section we first introduce the notion of synchronic dynamic behavior in a graph. If a graph, such as the spatial subgraphs studied in the present work (see Fig. 1), exhibits spatial synchronic coevolutionary dynamics, it will not show any sort of spatial variation in coevolutionary outcomes. Because geographic variation is a key aspect of the coevolutionary process (Thompson 2005), it is therefore relevant to assess the potential of a given spatial subgraph to exhibit synchronic behavior. Below, these notions are explained in detail. Second, it will be shown in the following sections how our Matching Alleles Model (see Methods) can be embedded in the Laplacian matrix framework of measuring synchrony potential by using equation (19), which is derived in the present section.

Let us consider *n* identical oscillators. Oscillators are systems that fluctuate in deterministic ways between two extreme values such as physical pendulums (Teschl 2012), Lotka-Volterra predator-prey systems (Hofbauer and Sigmund 1998), or synchronic masting oak trees (Koening and Knops 1998). The dynamics of the *i-th* oscillator is governed by:

$$x'_i(t) = F(\, x_i(t)\,)\,. \tag{16}$$

To simplify the notation $x_i(t) = x_i$, hereafter, with x_i being a function of time. Each oscillator represents a node in a graph. Oscillators are coupled if the dynamics in the *i-th* node affects the dynamics in all other nodes that are connected to it. A way of formalizing that coupling for the *i-th* node is:

$$x'_i = F(\, x_i) + \sigma \sum_j \alpha_{ij} \left(H(x_j) - H(x_i) \right), \tag{17}$$

where α_{ij} are elements of the associated *adjacency* matrix, σ is a parameter that specifies the strength of the coupling, and *F* and *H* are functions describing the dynamics of the oscillators considered (Barahona and Pecora 2002). Then (17) can be written as a function of the Laplacian matrix after some steps:

$$x'_i = F(x_i) + \sigma \sum_j \left[\alpha_{ij} H(x_j) - \alpha_{ij} H(x_i) \right]$$

$$\Leftrightarrow x'_i = F(x_i) + \sigma \left[\sum_j \alpha_{ij} H(x_j) - H(x_i) \sum_j \alpha_{ij} \right]. \quad (18)$$

Because $H(x_j) - H(x_i) = 0$ when $j=i$, it is possible to make the sums in (18) to be over all j but $j=i$, as the term does not contribute to the sum. Then, by noting that $\sum_j \alpha_{ij} = k_i$, equation (18) can be rewritten as follows:

$$x'_i = F(x_i) + \sigma \left[\left(\sum_j \alpha_{ij} H(x_j) \right) - H(x_i) k_i \right]$$

$$\Leftrightarrow x'_i = F(x_i) - \sigma \left[H(x_i) k_i - \sum_j a_{ij} H(x_j) \right]$$

$$\Leftrightarrow x'_i = F(x_i) - \sigma \sum_j l_{ij} H(x_j) \quad (19)$$

For equation (19) to exhibit fully synchronized behavior, we need that $x_i(t) = x^*(t), \forall i$, where $x^*(t)$ is a solution of the system. The local stability of the fully synchronized state in (19) can be studied through its *master stability function* (Barahona and Pecora 2002). This procedure yields that the higher the eigenratio $\lambda_2 / \lambda_{\max}$, the higher is the likelihood of synchronization. As the eigenratio decreases, so does the potential for exhibiting synchronized dynamics. Thus, the potential of a graph of exhibiting synchronized dynamics can be measured through the eigenratio $\lambda_2 / \lambda_{\max}$ associated to its Laplacian matrix.

iii) MAM as a time continuous oscillator

In this section we show that the spatially explicit Matching Alleles Model described in the main text (see Methods section) can be mapped into (19). Therefore, we can assess the potential of every given spatial subgraph – including larger networks not explored in our

study - to exhibit synchronized behavior. In other words, we can assess, for each spatial subgraph, whether they are prone to exhibit spatially invariable (synchronic) or spatially variable (asynchronous) coevolutionary dynamics by analyzing their Laplacian matrices.

To do so, we first explain how the MAM model can be written as a time-continuous oscillator. We will focus on the equations governing the dynamics of one allele of a single species to simplify the notation, but it is straightforward to extend the entire proof to *n*-species and alleles. First, we need to show that MAM dynamics can be mapped into oscillatory continuous-time models, such as the replicator equation:

$$x_i'(t) = x_i(t)[f_i(x) - \phi(x)], \tag{20}$$

where $x_i(t)$ is the frequency of allele *i* at time *t*, x is vector of all possible genetic frequencies (i.e. $x = (x_1,...,x_n)$), $f_i(x)$ is the fitness of allele x_i in the population, and $\phi(x)$ is the average population fitness (i.e. $\phi(x) = \sum_{j=1}^{n} x_j f_j(x)$) (Ohtsuki and Nowak 2006). To do so, let us take equation (2) of the online appendix and let us consider a spatial explicit version of it, where we specify the frequency of allele *X* of a given species in each site. Then equation (2) for the *i*-th site becomes:

$$X_i^{t+1} = \frac{X_i^t W_{Xt}}{X_i^t W_{Xt} + (1 - X_i^t) W_{xt}}, \tag{21}$$

where X_i^t is the frequency of allele *X* at time *t* and site *i*, W_{Xt} is the fitness for allele *X* at time *t*, and W_{xt} is the fitness of allele *x* at time *t* (see methods for a definition of fitness). As explained in section A of the online appendix, we can take the difference of the frequencies of two consecutive time steps as an estimate of the rate of change: $\Delta X_i = X_i^{t+1} - X_i^t$. This difference equation can be re-worked as:

$$\Delta X_i = \frac{X_i^t W_{Xt}}{X_i^t W_{Xt} + (1 - X_i^t) W_{xt}} - X_i^t$$

$$\Leftrightarrow \Delta X_i = X_i^t \left(\frac{W_{Xt}}{X_i^t W_{Xt} + (1 - X_i^t) W_{xt}} - 1 \right)$$

$$\Leftrightarrow \Delta X_i = \frac{X_i^t}{X_i^t W_{Xt} + (1 - X_i^t) W_{xt}} \left[W_{Xt} - \left(X_i^t W_{Xt} + (1 - X_i^t) W_{xt} \right) \right] \quad (22)$$

If we observe that $X_i^t W_{Xt} + (1 - X_i^t) W_{xt} = \phi$, the average population fitness, and that $W_{Xt} = f_i$, the fitness of allele X given the population, we can re-write (22) as: $\Delta X_i = \frac{X_i^t}{\phi} \left[f_X - \phi \right]$.

Because ϕ undergoes dampened oscillations as the system goes to equilibrium, the difference between equation (22) and (20) fades out too. At the equilibrium, (22) behaves exactly as (20), while away from the equilibrium the difference between the two is the scaling factor ϕ, which is known and varies deterministically. Thus, the time-discrete MAM model used in the main text can be mapped into a time-continuous oscillatory model as the replicator equation.

Next, we will show how this is still true when we consider gene flow across sites. To consider gene flow between sites, we use equation (7) of the main text (see Methods), so that the post-migration frequency of allele *X* at site *i* would be:

$$X_i^{t+1\ post-migration} = \sum_{j=1}^{n} M(i,j) X_j^{t+1} \quad (23)$$

Then, assuming that gene flow does not change with time, we can calculate the rate of change as follows:

$$\Delta X_i^{post-migration} = \sum_{j=1}^{n} M(i,j) X_j^{t+1} - \sum_{j=1}^{n} M(i,j) X_j^t$$

$$\Leftrightarrow \Delta X_i^{post-migration} = \sum_{j=1}^{n} M(i,j) \frac{X_j^t W_{Xt}}{X_j^t W_{Xt} + (1 - X_j^t) W_{xt}} - \sum_{j=1}^{n} M(i,j) X_j^t$$

$$\Leftrightarrow \Delta X_i^{post-migration} = \sum_{j=1}^{n} M(i,j) \left[\frac{X_j^t W_{Xt}}{X_j^t W_{Xt} + (1 - X_j^t) W_{xt}} - X_j^t \right]. \quad (24)$$

Equation (24) can be written as: $\overset{post-migration}{\Delta X_i} = \sum_{j=1}^{n} M(i,j)\frac{X_j^t}{\phi_j}\left[f_X - \phi_j\right]$, which is a weighted sum of scaled replicator equations. It is therefore safe to assume that the dynamics analyzed in the main text are described in continuous time by the following equation:

$$X_i'(t) = \sum_{j=1}^{n} M(i,j)\tilde{H}\left(X_j(t)\right), \tag{25}$$

where X_i is the frequency of allele X at time t and $\tilde{H}$ is a function that maintains the dynamic properties of (20), such as $\frac{X_j^t}{\phi_j}\left[f_X - \phi_j\right]$, the scaled replicator equation.

iv) Writing the time-continuous MAM as a function of the Laplacian matrix

In this section we show that it is possible to rewrite equation (25) (i.e. time continuous MAM) as equation (19), and hence, as a function of the Laplacian matrix. By doing so, we show that we can analyze the potential of each spatial subgraph to exhibit spatially varying coevolutionary dynamics. We will first focus on the binary structure of the spatial subgraphs, and then we will extend our method to the weighted structure, i.e. the spatial subgraphs considering gene flow between sites.

Let us start by observing that $M(i,j)$ can be written as a weighted adjacency matrix such that $M(i,j) = \alpha_{ij}\varpi_{ij}$ (similar as in Nishikawa and Motter 2006), where α_{ij} is an element of the adjacency matrix and ϖ_{ij} is a weight, here, gene flow magnitude. Now we focus in the case where all weights are equal to 1, so that $M(i,j) = \alpha_{ij}$, and thus only considers the binary structure of the spatial subgraphs. In this case, equation (25) can be written as:

$$X_i' = \sum_{j=1}^{n} \alpha_{ij}\tilde{H}\left(X_j\right). \tag{26}$$

We can now rewrite equation (26) as (19):

$$X_i' = \sum_{j=1}^{n} \alpha_{ij} \left[\tilde{H}\left(X_j\right) - \tilde{H}\left(X_i\right) + \tilde{H}\left(X_i\right) \right] \tag{27}$$

$$\Leftrightarrow X_i' = \sum_{j=1}^{n} \alpha_{ij} \left[\tilde{H}\left(X_j\right) - \tilde{H}\left(X_i\right) \right] + \overbrace{\sum_{j=1}^{n} \alpha_{ij} \tilde{H}\left(X_i\right)}^{\tilde{F}(X_i)} \tag{28}$$

Equation (28) has the same functional form than equation (17), and can thus be rewritten as equation (19):

$$X_i' = \tilde{F}(X_i) - \sum_{j=1}^{n} l_{ij} \tilde{H}\left(X_j\right), \tag{29}$$

where l_{ij} is an element of the Laplacian matrix L, where $l_{ij} = -\alpha_{ij}$ and. We have therefore shown that the synchronizability of the MAM model can be assessed through the binary Laplacian matrix of the spatial subgraphs when gene flow is constant across all sites and equal to 1.

Next we will extend the same argument to weighted Laplacian matrices, which can thus take gene flow between sites into account. To do so, we can think about the gene flow matrix, $M(i,j)$, as a weighted adjacency matrix. Basically, it is a gene flow magnitude times 1 when two sites are connected, or 0, when two sites are not connected. Formally: $M(i,j) = \alpha_{ij} \varpi_{ij}$. Then, equation (26) becomes:

$$X_i' = \sum_{j=1}^{n} \alpha_{ij} \varpi_{ij} \tilde{H}\left(X_j\right). \tag{30}$$

And we follow a similar procedure than with equation (26), such that (30) can be rewritten as:

$$X_i' = \alpha_{ij} \varpi_{ij} \tilde{H}\left(X_i\right) + \sum_{\substack{j=1 \\ j \neq i}}^{n} \alpha_{ij} \varpi_{ij} \left[\tilde{H}\left(X_j\right) - \tilde{H}\left(X_i\right) + \tilde{H}\left(X_i\right) \right]. \tag{31}$$

Note that compared to (27), the only change (besides the fact that we are considering weights), is that we are explicitly taking the dynamics of the focal node *i* out of the sum. We can rewrite (31) as:

$$X_i' = \alpha_{ij}\varpi_{ij}\tilde{H}\left(X_i\right) + \sum_{\substack{j=1 \\ j\neq i}}^{n} \alpha_{ij}\varpi_{ij}\left[\tilde{H}\left(X_j\right) - \tilde{H}\left(X_i\right)\right] + \sum_{\substack{j=1 \\ j\neq i}}^{n} \alpha_{ij}\varpi_{ij}\tilde{H}\left(X_i\right)$$

$$\Leftrightarrow X_i' = \overbrace{\sum_{j=1}^{n} \alpha_{ij}\varpi_{ij}\tilde{H}\left(X_i\right)}^{\hat{F}(X_i)} + \sum_{\substack{j=1 \\ j\neq i}}^{n} \alpha_{ij}\varpi_{ij}\left[\tilde{H}\left(X_j\right) - \tilde{H}\left(X_i\right)\right]$$

$$X_i' = \hat{F}(X_i) - \sum_{j=1}^{n} \hat{l}_{ij}\tilde{H}\left(X_j\right), \tag{32}$$

where $\hat{F}$ is a function that has the same dynamic properties than F and $\tilde{F}$, but takes into account gene flow, and $\hat{l}_{ij} = -\alpha_{ij}\varpi_{ij}$ and $\hat{l}_{ii} = \sum_{j\neq i}^{n} \alpha_{ij}\varpi_{ij}$ (similar to what Nishikawa and Motter 2006, have found). We have therefore shown that we can use both the binary (non-weighted) Laplacian matrix and weighted (taking gene flow into account) Laplacian matrix associated to each spatial subgraph to assess how prone they are to exhibit spatially varying coevolutionary dynamics.

v) Assessing synchronizability using the binary structure of spatial subgraphs

In this section we analyze how prone each of the four spatial subgraphs analyzed in the main text (i.e. star, cycle, linear and modular) are to exhibit spatially varying coevolutionary dynamics. If they are highly synchronizable, they are less prone to exhibit spatially variable coevolutionary dynamics. The Laplacian matrices for each structure are (note that $L = \mathbf{D} - \mathbf{A}$):

$$L_{star} = \begin{pmatrix} 5 & -1 & -1 & -1 & -1 & -1 \\ -1 & 1 & 0 & 0 & 0 & 0 \\ -1 & 0 & 1 & 0 & 0 & 0 \\ -1 & 0 & 0 & 1 & 0 & 0 \\ -1 & 0 & 0 & 0 & 1 & 0 \\ -1 & 0 & 0 & 0 & 0 & 1 \end{pmatrix}, \tag{33}$$

$$L_{cycle} = \begin{pmatrix} 2 & -1 & 0 & 0 & 0 & -1 \\ -1 & 2 & -1 & 0 & 0 & 0 \\ 0 & -1 & 2 & -1 & 0 & 0 \\ 0 & 0 & -1 & 2 & -1 & 0 \\ 0 & 0 & 0 & -1 & 2 & -1 \\ -1 & 0 & 0 & 0 & -1 & 2 \end{pmatrix}, \tag{34}$$

$$L_{linear} = \begin{pmatrix} 1 & -1 & 0 & 0 & 0 & 0 \\ -1 & 2 & -1 & 0 & 0 & 0 \\ 0 & -1 & 2 & -1 & 0 & 0 \\ 0 & 0 & -1 & 2 & -1 & 0 \\ 0 & 0 & 0 & -1 & 2 & -1 \\ 0 & 0 & 0 & 0 & -1 & 1 \end{pmatrix}, \tag{35}$$

$$L_{\mathrm{mod}ular} = \begin{pmatrix} 3 & -1 & -1 & -1 & 0 & 0 \\ -1 & 2 & -1 & 0 & 0 & 0 \\ -1 & -1 & 2 & 0 & 0 & 0 \\ -1 & 0 & 0 & 3 & -1 & -1 \\ 0 & 0 & 0 & -1 & 2 & -1 \\ 0 & 0 & 0 & -1 & -1 & 2 \end{pmatrix}. \tag{36}$$

For each case, we calculated the eigenratio $\lambda_2 / \lambda_{\max}$, and ranked the spatial structures according to their proneness to exhibit spatial variation in coevolutionary dynamics (Table B1). If the eigenratio is closer to 1, then the spatial structure is highly synchronizable and hence less prone to exhibit spatially variable coevolutionary dynamics. If the eigenratio is closer to 0, the spatial structure is poorly synchronizable and hence more prone to exhibit spatial variation in coevolutionary dynamics.

Our results suggest that the likelihood of spatially variable coevolutionary dynamics at a network scale is maximal for the linear and modular structures, and is minimal for the star and cycle. The results at the network level dynamics are consistent to a great extent with the results at the local level (within sites). At a local level, we observed that higher gene flow promotes synchronized dynamics between contiguous sites (see online appendix C). This local synchronization can cascade up with time, eventually leading to synchronization of the entire network. The latter was observed at high gene flow levels, where unstable dynamics of

the hotspot cascade throughout the entire subgraph, leading to a network level synchronic unstable state (online appendix C). Hence, the unstable region at high levels of gene flow in fig. 2 (high σ) is characterized by unstable oscillatory dynamics where synchronization is likely and common (online appendix C). The size of this unstable region can thus be considered as proxy for the likelihood of a given subgraph to exhibit spatially variable coevolutionary dynamics.

The results of the binary Laplacian matrix are thus largely consistent with our simulations (see Table B1 and fig. 2 of main text). Departures of some of our simulations from these theoretical predictions can be explained by the idiosyncratic effect of hotspot position and hotspot connectivity. For example, if we consider the star structure with peripheral hotspot, our simulation results match perfectly well the predictions of the binary Laplacian matrix. However, these predictions do not hold for the star structure with central hotspot, as it seems to be more prone to synchronize than the cycle. Inferences based on the Laplacian matrix often focuses on the dynamics among sites but in some situations the effects due to the differences in the dynamics within sites (e.g., coldspots vs. hotspots) would lead to departures to the predictions derived from the Laplacian matrices. Therefore, although the Laplacian matrix can accurately predict the global likelihood for a given subgraph to exhibit spatially variable coevolutionary dynamics, there are situations in which the assumption of site equivalence is crucial and the analytic predictions deviate from the simulation results. Thus, it is always paramount to take into account the factors described in the main text as major drivers of coevolution and combine information of hotspot connectivity, hotspot centrality and the spatial configuration of coldspots.

Two questions still remain. First, what would happen to the predictions of the binary Laplacian matrix if we consider spatial structures with more than 6 sites? Second, what would

happen to these predictions if we consider the magnitude of gene flow between sites, instead of only their binary structure? Both questions are answered in the following two sections.

Table B1: Eigenratio for each subgraph and likelihood of exhibiting spatially variable coevolutionary dynamics.

	EigenRatio $\left(\frac{\lambda_2}{\lambda_{max}}\right)$	Predicted likelihood of spatially variable coevolutionary dynamics
Cycle	0.250	Very unlikely
Star	0.170	
Modular	0.096	
Linear	0.072	Very likely

vi) Assessing the effect of site addition upon Laplacian predictions

In this section we show that the predictions of the binary Laplacian matrix are in general robust to variations in the number of sites. To do so, we first added more sites to each subgraph in such a way that it would not affect the general structure of the graph. In the star, we connected more sites to the hotspot, in a way similar to fig. 4-A to E of the main text. For the cycle, we just considered cycles with higher number of sites (i.e., 7-cycle, 8-cycle and so on). For the linear structure, we connected sites to one of the ends of the structure, in a way similar to fig. 4-F to G of the main text. Because the modular structure is not a regular graph such as the star, the cycle and the linear, site-addition can occur either in the modules (fig. B1-A), or in the connection between modules (fig. B1-B). We explored both scenarios, and calculated the eigenratio $\lambda_2 / \lambda_{max}$ of the binary Laplacian matrix for each of the resulting structures and number of sites (fig. B2).

It can be seen that as the number of sites increase, the eigenratios decrease, but the curves rarely cross each other (fig. 6). First, this indicates the larger the number of sites, the lower is the likelihood of synchronization. Second, and more importantly, these results suggest that the predictions of the binary Laplacian matrix are in general robust to variations

in the number of sites. Nevertheless, the eigenratio of the star structure becomes larger than that of the cycle after they reached a size of approximately 10 sites. Finally, depending on where sites are added, the likelihood of the modular structure to exhibit spatially varying coevolutionary dynamics changes. When sites are added to each module, the likelihood remains different to that of a linear subgraph. When sites are added to the connection between modules, the likelihood becomes more and more similar to that of a linear structure. This result highlights the importance of the spatial configuration of coldspots in the overall spatial structure.

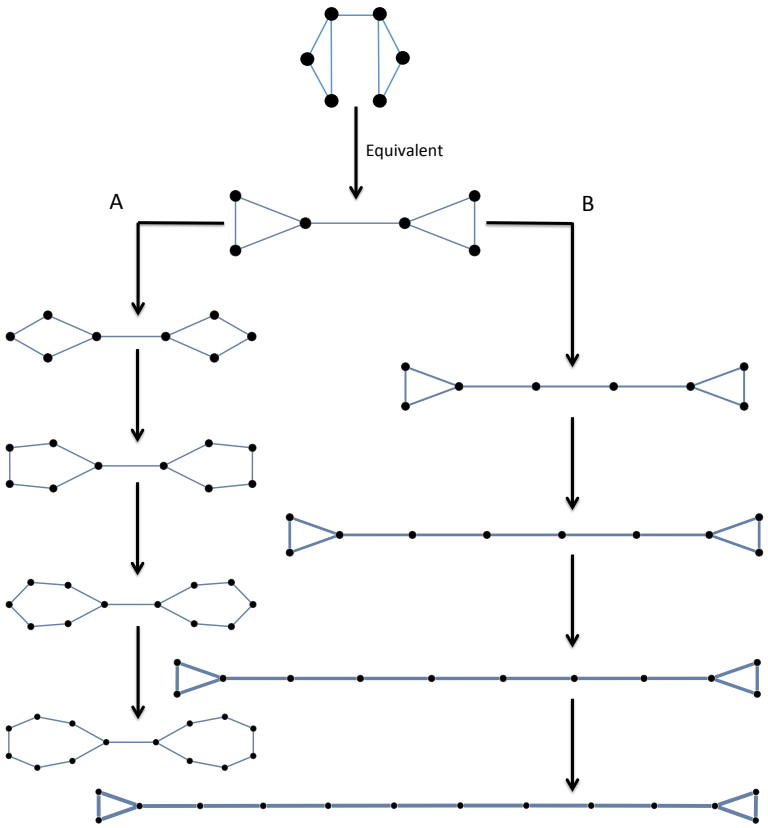

Figure B1: The two possible procedures of site addition are depicted for the modular subgraph. **A.** Site addition by module enlargement (called Modular-C, because each module is a cycle). B. Site addition by enlargement of the connection between modules (calles Modular-L, because as the connection between modules gets enlarged, it the whole structure becomes more and more similar to a linear subgraph).

vii) Assessing synchronizability using spatial subgraphs and information on gene flow

In this section we show that using the Laplacian method solely based on the binary structure of a spatial subgraph is sufficient to make accurate predictions on the likelihood of a given spatial subgraph to exhibit spatially variable coevolutionary dynamics. Although considering gene flow between sites may be relevant for making quantitative predictions, these can be adequately estimated from the binary structure, which has important implications for testing our ideas in the field.

To do so, we use the previously derived equation (32) (see section iv) to incorporate gene flow magnitudes to the Laplacian matrices associated to each spatial subgraph. Equation (32) shows that $l_{ij} = -\alpha_{ij}\varpi_{ij}$ and $l_{ii} = \sum_{j\neq 1}^{n} \alpha_{ij}\varpi_{ij}$, where ϖ_{ij} is the gene flow between sites i and j, or M(i,j), defined as $M(i,j) = \dfrac{\exp\left[-\frac{1}{2}\left(\frac{d_{ij}}{\sigma}\right)^2\right]}{\sum_{j=1}^{n}\exp\left[-\frac{1}{2}\left(\frac{d_{ij}}{\sigma}\right)^2\right]}$. Then, we obtain:

$$L_{star} = \begin{pmatrix} \frac{5e^{-\frac{1}{2\sigma^2}}}{1+5e^{-\frac{1}{2\sigma^2}}} & -\frac{e^{-\frac{1}{2\sigma^2}}}{1+5e^{-\frac{1}{2\sigma^2}}} & -\frac{e^{-\frac{1}{2\sigma^2}}}{1+5e^{-\frac{1}{2\sigma^2}}} & -\frac{e^{-\frac{1}{2\sigma^2}}}{1+5e^{-\frac{1}{2\sigma^2}}} & -\frac{e^{-\frac{1}{2\sigma^2}}}{1+5e^{-\frac{1}{2\sigma^2}}} & -\frac{e^{-\frac{1}{2\sigma^2}}}{1+5e^{-\frac{1}{2\sigma^2}}} \\ -\frac{e^{-\frac{1}{2\sigma^2}}}{1+e^{-\frac{1}{2\sigma^2}}} & \frac{e^{-\frac{1}{2\sigma^2}}}{1+e^{-\frac{1}{2\sigma^2}}} & 0 & 0 & 0 & 0 \\ -\frac{e^{-\frac{1}{2\sigma^2}}}{1+e^{-\frac{1}{2\sigma^2}}} & 0 & \frac{e^{-\frac{1}{2\sigma^2}}}{1+e^{-\frac{1}{2\sigma^2}}} & 0 & 0 & 0 \\ -\frac{e^{-\frac{1}{2\sigma^2}}}{1+e^{-\frac{1}{2\sigma^2}}} & 0 & 0 & \frac{e^{-\frac{1}{2\sigma^2}}}{1+e^{-\frac{1}{2\sigma^2}}} & 0 & 0 \\ -\frac{e^{-\frac{1}{2\sigma^2}}}{1+e^{-\frac{1}{2\sigma^2}}} & 0 & 0 & 0 & \frac{e^{-\frac{1}{2\sigma^2}}}{1+e^{-\frac{1}{2\sigma^2}}} & 0 \\ -\frac{e^{-\frac{1}{2\sigma^2}}}{1+e^{-\frac{1}{2\sigma^2}}} & 0 & 0 & 0 & 0 & \frac{e^{-\frac{1}{2\sigma^2}}}{1+e^{-\frac{1}{2\sigma^2}}} \end{pmatrix}, \quad (37)$$

$$L_{cycle} = \begin{pmatrix} \frac{2e^{-\frac{1}{2\sigma^2}}}{1+2e^{-\frac{1}{2\sigma^2}}} & -\frac{e^{-\frac{1}{2\sigma^2}}}{1+2e^{-\frac{1}{2\sigma^2}}} & 0 & 0 & 0 & -\frac{e^{-\frac{1}{2\sigma^2}}}{1+2e^{-\frac{1}{2\sigma^2}}} \\ -\frac{e^{-\frac{1}{2\sigma^2}}}{1+2e^{-\frac{1}{2\sigma^2}}} & \frac{2e^{-\frac{1}{2\sigma^2}}}{1+2e^{-\frac{1}{2\sigma^2}}} & -\frac{e^{-\frac{1}{2\sigma^2}}}{1+2e^{-\frac{1}{2\sigma^2}}} & 0 & 0 & 0 \\ 0 & -\frac{e^{-\frac{1}{2\sigma^2}}}{1+2e^{-\frac{1}{2\sigma^2}}} & \frac{2e^{-\frac{1}{2\sigma^2}}}{1+2e^{-\frac{1}{2\sigma^2}}} & -\frac{e^{-\frac{1}{2\sigma^2}}}{1+2e^{-\frac{1}{2\sigma^2}}} & 0 & 0 \\ 0 & 0 & -\frac{e^{-\frac{1}{2\sigma^2}}}{1+2e^{-\frac{1}{2\sigma^2}}} & \frac{2e^{-\frac{1}{2\sigma^2}}}{1+2e^{-\frac{1}{2\sigma^2}}} & -\frac{e^{-\frac{1}{2\sigma^2}}}{1+2e^{-\frac{1}{2\sigma^2}}} & 0 \\ 0 & 0 & 0 & -\frac{e^{-\frac{1}{2\sigma^2}}}{1+2e^{-\frac{1}{2\sigma^2}}} & \frac{2e^{-\frac{1}{2\sigma^2}}}{1+2e^{-\frac{1}{2\sigma^2}}} & -\frac{e^{-\frac{1}{2\sigma^2}}}{1+2e^{-\frac{1}{2\sigma^2}}} \\ -\frac{e^{-\frac{1}{2\sigma^2}}}{1+2e^{-\frac{1}{2\sigma^2}}} & 0 & 0 & 0 & -\frac{e^{-\frac{1}{2\sigma^2}}}{1+2e^{-\frac{1}{2\sigma^2}}} & \frac{2e^{-\frac{1}{2\sigma^2}}}{1+2e^{-\frac{1}{2\sigma^2}}} \end{pmatrix}, \tag{38}$$

$$L_{linear} = \begin{pmatrix} \frac{e^{-\frac{1}{2\sigma^2}}}{1+e^{-\frac{1}{2\sigma^2}}} & -\frac{e^{-\frac{1}{2\sigma^2}}}{1+e^{-\frac{1}{2\sigma^2}}} & 0 & 0 & 0 & 0 \\ -\frac{e^{-\frac{1}{2\sigma^2}}}{1+2e^{-\frac{1}{2\sigma^2}}} & \frac{2e^{-\frac{1}{2\sigma^2}}}{1+2e^{-\frac{1}{2\sigma^2}}} & -\frac{e^{-\frac{1}{2\sigma^2}}}{1+2e^{-\frac{1}{2\sigma^2}}} & 0 & 0 & 0 \\ 0 & -\frac{e^{-\frac{1}{2\sigma^2}}}{1+2e^{-\frac{1}{2\sigma^2}}} & \frac{2e^{-\frac{1}{2\sigma^2}}}{1+2e^{-\frac{1}{2\sigma^2}}} & -\frac{e^{-\frac{1}{2\sigma^2}}}{1+2e^{-\frac{1}{2\sigma^2}}} & 0 & 0 \\ 0 & 0 & -\frac{e^{-\frac{1}{2\sigma^2}}}{1+2e^{-\frac{1}{2\sigma^2}}} & \frac{2e^{-\frac{1}{2\sigma^2}}}{1+2e^{-\frac{1}{2\sigma^2}}} & -\frac{e^{-\frac{1}{2\sigma^2}}}{1+2e^{-\frac{1}{2\sigma^2}}} & 0 \\ 0 & 0 & 0 & -\frac{e^{-\frac{1}{2\sigma^2}}}{1+2e^{-\frac{1}{2\sigma^2}}} & \frac{2e^{-\frac{1}{2\sigma^2}}}{1+2e^{-\frac{1}{2\sigma^2}}} & -\frac{e^{-\frac{1}{2\sigma^2}}}{1+2e^{-\frac{1}{2\sigma^2}}} \\ 0 & 0 & 0 & 0 & -\frac{e^{-\frac{1}{2\sigma^2}}}{1+e^{-\frac{1}{2\sigma^2}}} & \frac{e^{-\frac{1}{2\sigma^2}}}{1+e^{-\frac{1}{2\sigma^2}}} \end{pmatrix}, \tag{39}$$

$$L_{modular} = \begin{pmatrix} \frac{3e^{-\frac{1}{2\sigma^2}}}{1+3e^{-\frac{1}{2\sigma^2}}} & -\frac{e^{-\frac{1}{2\sigma^2}}}{1+3e^{-\frac{1}{2\sigma^2}}} & -\frac{e^{-\frac{1}{2\sigma^2}}}{1+3e^{-\frac{1}{2\sigma^2}}} & -\frac{e^{-\frac{1}{2\sigma^2}}}{1+3e^{-\frac{1}{2\sigma^2}}} & 0 & 0 \\ -\frac{e^{-\frac{1}{2\sigma^2}}}{1+2e^{-\frac{1}{2\sigma^2}}} & \frac{2e^{-\frac{1}{2\sigma^2}}}{1+2e^{-\frac{1}{2\sigma^2}}} & -\frac{e^{-\frac{1}{2\sigma^2}}}{1+2e^{-\frac{1}{2\sigma^2}}} & 0 & 0 & 0 \\ -\frac{e^{-\frac{1}{2\sigma^2}}}{1+2e^{-\frac{1}{2\sigma^2}}} & -\frac{e^{-\frac{1}{2\sigma^2}}}{1+2e^{-\frac{1}{2\sigma^2}}} & \frac{2e^{-\frac{1}{2\sigma^2}}}{1+2e^{-\frac{1}{2\sigma^2}}} & 0 & 0 & 0 \\ -\frac{e^{-\frac{1}{2\sigma^2}}}{1+3e^{-\frac{1}{2\sigma^2}}} & 0 & 0 & \frac{3e^{-\frac{1}{2\sigma^2}}}{1+3e^{-\frac{1}{2\sigma^2}}} & -\frac{e^{-\frac{1}{2\sigma^2}}}{1+3e^{-\frac{1}{2\sigma^2}}} & -\frac{e^{-\frac{1}{2\sigma^2}}}{1+3e^{-\frac{1}{2\sigma^2}}} \\ 0 & 0 & 0 & -\frac{e^{-\frac{1}{2\sigma^2}}}{1+2e^{-\frac{1}{2\sigma^2}}} & \frac{2e^{-\frac{1}{2\sigma^2}}}{1+2e^{-\frac{1}{2\sigma^2}}} & -\frac{e^{-\frac{1}{2\sigma^2}}}{1+2e^{-\frac{1}{2\sigma^2}}} \\ 0 & 0 & 0 & -\frac{e^{-\frac{1}{2\sigma^2}}}{1+2e^{-\frac{1}{2\sigma^2}}} & -\frac{e^{-\frac{1}{2\sigma^2}}}{1+2e^{-\frac{1}{2\sigma^2}}} & \frac{2e^{-\frac{1}{2\sigma^2}}}{1+2e^{-\frac{1}{2\sigma^2}}} \end{pmatrix}. \quad (40)$$

We can now calculate the eigenratio $\lambda_2 / \lambda_{\max}$ for each of the subgraphs as a function of σ. Our results suggest that the predictions made by the quantitative Laplacian matrix show some deviances from those made by the binary Laplacian matrix (fig. 6). Nevertheless, these differences are in general small, rapidly reaching asymptotic values, suggesting that the predictions made by the binary Laplacian matrix are good qualitative estimates of those made by the Laplacian matrix that considers gene flow between sites.

viii) The Laplacian matrix as a predictor for local dynamics.

If the Laplacian matrix is a good predictor of global, network-scale dynamics it should also be a good predictor for local dynamics. Although the latter may be affected by hotspot connectivity, coldspot configuration and distance to hotspot, if the entire network is able to maintain polymorphisms, then each site should also be able to do so. A plot of the asymptotic eigenratio of the analyzed spatial subgraphs with infinite amount of sites against the probability of stable dynamics in the hotspots shows a one-to-one relationship (fig. B2). Thus, as suggested by the theory of diffusion in networks, we found that smaller eigenratios are associated with larger probabilities of stable dynamics, and the Laplacian matrices are indeed

good estimators of local coevolutionary dynamics, as well as of global, network-scale coevolutionary dynamics.

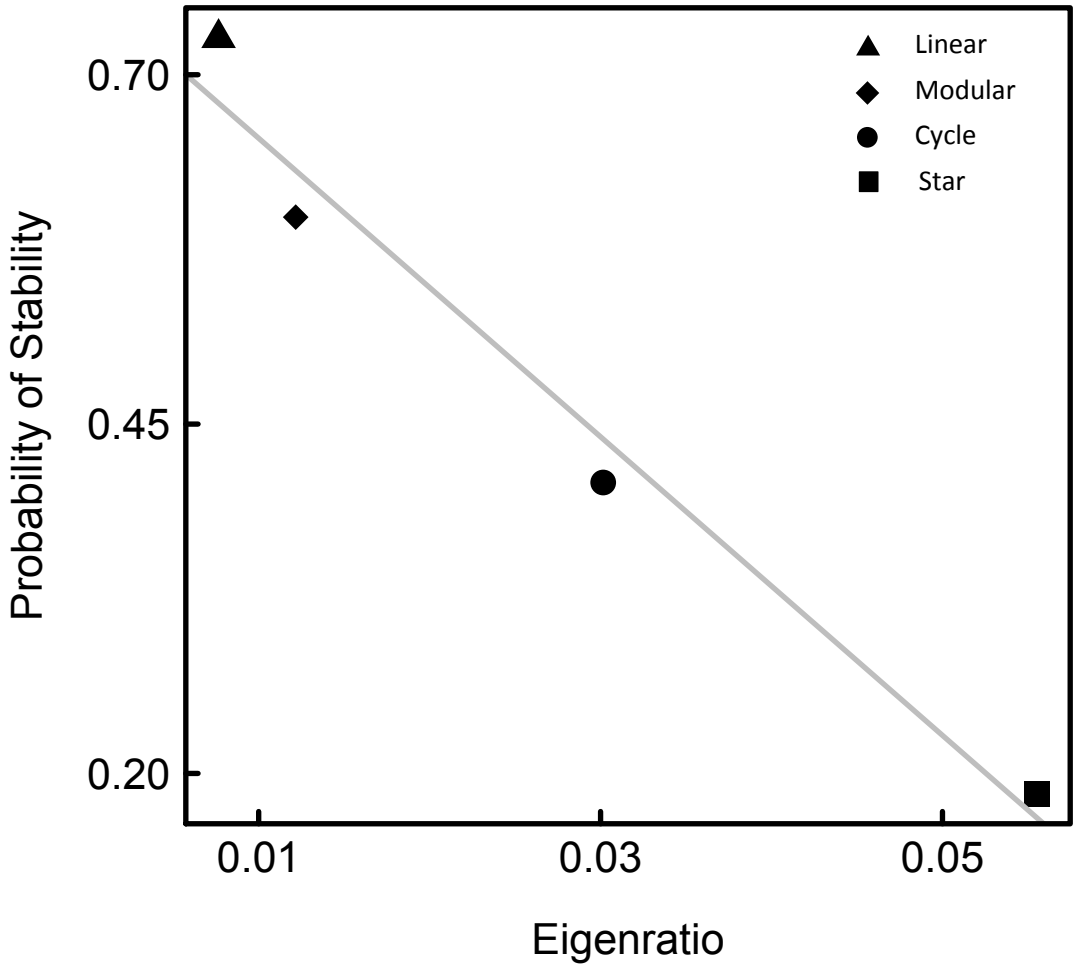

Figure B2: Plot of mean Probability of Stable coevolutionary dynamics in the hotspot against asymptotic Eigenratio of each of the four different considered spatial networks. Note hotspot centrality does not affect Laplacian matrices. For the asymptotic eigenratio of the modular spatial network, we took the mean of the two possible versions, Modular-C and Modular-L (Figure B1). It can be seen that as the eigenratio increases, the probability of having stable, synchronic coevolutionary dynamics decreases. These stable synchronic dynamics yield in turn polymorphic populations. Hence, increased eigenratio yields a smaller probability of maintaining polymorphisms and showing spatially varying coevolutionary dynamics.

C) How to use the Laplacian matrix in real systems

i) Parameterizing the Laplacian with real data:

To use the Laplacian matrices of real spatial networks to either test our results, or predict possible future coevolutionary dynamics, it would be necessary to gather information on: (1) the number of sites the landscape is divided in, and (2) the magnitude of gene flow between each pair of sites, or at least whether gene flow occurs, or not. One possible way to estimate gene flow is using:

$$Nm = \frac{1 - F_{st}}{4F_{st}}, \tag{41}$$

where Nm is the number of individual migrants per generation, and F_{st} is Wright's measure of population differentiation due to genetic structure, which can conveniently be estimated from genetic polymorphism data (Cockerham and Weir 1993). However, other possible ways to measure gene flow are also available (see Holsinger and Weir 2009 for a review of them). Assuming this information can be gathered, it would be possible to proceed with the parameterization of the Laplacian matrix of the system.

First, we need to depict the spatial network as an adjacency matrix (see (13) of the online appendix). Because we do not consider direction, the matrix is symmetric:

$$A = \begin{pmatrix}
0 & 1 & 1 & 1 & 1 & 1 & 1 & 1 & 1 & 1 & 1 & 1 & 1 & 1 \\
1 & 0 & 1 & 0 & 0 & 0 & 0 & 0 & 0 & 0 & 0 & 0 & 0 & 1 \\
1 & 1 & 0 & 1 & 0 & 0 & 0 & 0 & 0 & 0 & 0 & 0 & 0 & 0 \\
1 & 0 & 1 & 0 & 1 & 0 & 0 & 0 & 0 & 0 & 0 & 0 & 0 & 0 \\
1 & 0 & 0 & 1 & 0 & 1 & 0 & 0 & 0 & 0 & 0 & 0 & 0 & 0 \\
1 & 0 & 0 & 0 & 1 & 0 & 1 & 0 & 0 & 0 & 0 & 0 & 0 & 0 \\
1 & 0 & 0 & 0 & 0 & 1 & 0 & 1 & 0 & 0 & 0 & 0 & 0 & 0 \\
1 & 0 & 0 & 0 & 0 & 0 & 1 & 0 & 1 & 0 & 0 & 0 & 0 & 0 \\
1 & 0 & 0 & 0 & 0 & 0 & 0 & 1 & 0 & 1 & 0 & 0 & 0 & 0 \\
1 & 0 & 0 & 0 & 0 & 0 & 0 & 0 & 1 & 0 & 1 & 0 & 0 & 0 \\
1 & 0 & 0 & 0 & 0 & 0 & 0 & 0 & 0 & 1 & 0 & 1 & 0 & 0 \\
1 & 0 & 0 & 0 & 0 & 0 & 0 & 0 & 0 & 0 & 1 & 0 & 1 & 0 \\
1 & 0 & 0 & 0 & 0 & 0 & 0 & 0 & 0 & 0 & 0 & 1 & 0 & 1 \\
1 & 1 & 0 & 0 & 0 & 0 & 0 & 0 & 0 & 0 & 0 & 0 & 1 & 0
\end{pmatrix}. \tag{41}$$

The associated binary Laplacian matrix, $\boldsymbol{L}$, for the above adjacency matrix is defined by $L = \mathbf{D} - \mathbf{A}$, where $\mathbf{D}$ is the degree matrix (see eq. (14) of the online appendix). Thus, the binary Laplacian matrix is:

$$L_{binary} = \begin{pmatrix} 13 & -1 & -1 & -1 & -1 & -1 & -1 & -1 & -1 & -1 & -1 & -1 & -1 & -1 \\ -1 & 3 & -1 & 0 & 0 & 0 & 0 & 0 & 0 & 0 & 0 & 0 & 0 & -1 \\ -1 & -1 & 3 & -1 & 0 & 0 & 0 & 0 & 0 & 0 & 0 & 0 & 0 & 0 \\ -1 & 0 & -1 & 3 & -1 & 0 & 0 & 0 & 0 & 0 & 0 & 0 & 0 & 0 \\ -1 & 0 & 0 & -1 & 3 & -1 & 0 & 0 & 0 & 0 & 0 & 0 & 0 & 0 \\ -1 & 0 & 0 & 0 & -1 & 3 & -1 & 0 & 0 & 0 & 0 & 0 & 0 & 0 \\ -1 & 0 & 0 & 0 & 0 & -1 & 3 & -1 & 0 & 0 & 0 & 0 & 0 & 0 \\ -1 & 0 & 0 & 0 & 0 & 0 & -1 & 3 & -1 & 0 & 0 & 0 & 0 & 0 \\ -1 & 0 & 0 & 0 & 0 & 0 & 0 & -1 & 3 & -1 & 0 & 0 & 0 & 0 \\ -1 & 0 & 0 & 0 & 0 & 0 & 0 & 0 & -1 & 3 & -1 & 0 & 0 & 0 \\ -1 & 0 & 0 & 0 & 0 & 0 & 0 & 0 & 0 & -1 & 3 & -1 & 0 & 0 \\ -1 & 0 & 0 & 0 & 0 & 0 & 0 & 0 & 0 & 0 & -1 & 3 & -1 & 0 \\ -1 & 0 & 0 & 0 & 0 & 0 & 0 & 0 & 0 & 0 & 0 & -1 & 3 & -1 \\ -1 & -1 & 0 & 0 & 0 & 0 & 0 & 0 & 0 & 0 & 0 & 0 & -1 & 3 \end{pmatrix}. \quad (41)$$

Using real data, one could now calculate the eigenratio of the binary Laplacian matrix for the spatial network in fig. C1 (fig C2). Second, we can now incorporate the information available in fig.C1 with respect to gene flow, in a weighted adjacency matrix, by substituting the 1s for the actual value of gene flow between each pair of sites (dots depicting zeros to improve visualization):

$$A_{weighted} = \begin{pmatrix} . & .2 & .2 & .3 & .5 & .2 & .2 & .3 & .3 & .3 & .2 & .2 & .2 & .2 \\ .2 & . & .8 & . & . & . & . & . & . & . & . & . & . & .5 \\ .2 & .8 & . & .1 & . & . & . & . & . & . & . & . & . & . \\ .3 & . & .1 & . & .2 & . & . & . & . & . & . & . & . & . \\ .5 & . & . & .2 & . & .2 & . & . & . & . & . & . & . & . \\ .2 & . & . & . & .2 & . & .2 & . & . & . & . & . & . & . \\ .2 & . & . & . & . & .2 & . & .3 & . & . & . & . & . & . \\ .3 & . & . & . & . & . & .3 & . & .9 & . & . & . & . & . \\ .3 & . & . & . & . & . & . & .9 & . & .2 & . & . & . & . \\ .3 & . & . & . & . & . & . & . & .2 & . & .3 & . & . & . \\ .2 & . & . & . & . & . & . & . & . & .3 & . & .3 & . & . \\ .2 & . & . & . & . & . & . & . & . & . & .3 & . & .4 & . \\ .2 & . & . & . & . & . & . & . & . & . & . & .4 & . & .4 \\ .2 & .5 & . & . & . & . & . & . & . & . & . & . & .4 & . \end{pmatrix}. \quad (42)$$

To calculate the weighted Laplacian matrix, we first multiply all elements of the weighted adjacency matrix by -1. Then, we substitute each diagonal element with the sum of the absolute value of all elements in its respective row yielding:

$$L_{weight} = \begin{pmatrix} 3.3 & -.2 & -.2 & -.3 & -.5 & -.2 & -.2 & -.3 & -.3 & -.3 & -.2 & -.2 & -.2 & -.2 \\ -.2 & 1.5 & -.8 & . & . & . & . & . & . & . & . & . & . & -.5 \\ -.2 & -.8 & 1.1 & -.1 & . & . & . & . & . & . & . & . & . & . \\ -.3 & . & -.1 & 0.6 & -.2 & . & . & . & . & . & . & . & . & . \\ -.5 & . & . & -.2 & 0.9 & -.2 & . & . & . & . & . & . & . & . \\ -.2 & . & . & . & -.2 & 0.6 & -.2 & . & . & . & . & . & . & . \\ -.2 & . & . & . & . & -.2 & 0.7 & -.3 & . & . & . & . & . & . \\ -.3 & . & . & . & . & . & -.3 & 1.5 & -.9 & . & . & . & . & . \\ -.3 & . & . & . & . & . & . & -.9 & 1.4 & -.2 & . & . & . & . \\ -.3 & . & . & . & . & . & . & . & -.2 & 0.8 & -.3 & . & . & . \\ -.2 & . & . & . & . & . & . & . & . & -.3 & 0.8 & -.3 & . & . \\ -.2 & . & . & . & . & . & . & . & . & . & -.3 & 0.9 & -.4 & . \\ -.2 & . & . & . & . & . & . & . & . & . & . & -.4 & 1 & -.4 \\ -.2 & -.5 & . & . & . & . & . & . & . & . & . & . & -.4 & 1.1 \end{pmatrix} .(43)$$

Using the weighted Laplacian matrix it is possible to calculate the eigenratio, and compare it with the binary one (fig. 6-A, of the main text).

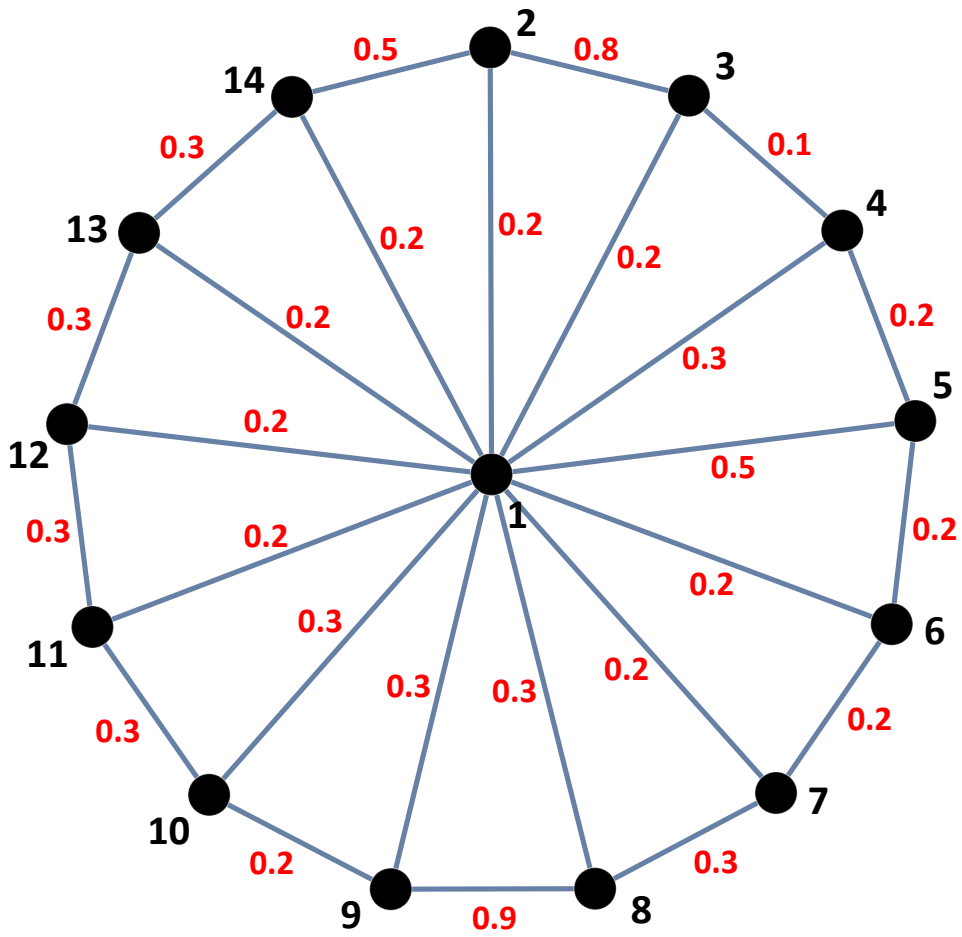

Figure C1: Hypothetical example of an "observed" spatial network to show how to parameterize the Laplacian matrix with real data. Black dots depict sites (identified by black numbers) and blue lines depict the existence of gene flow between sites. Red numbers quantify the amount of gene flow between pairs of sites.

D) Laplacian matrix in networks with varying levels of gene flow

i) Inferences from a simpler scenario

Testing how varying levels of gene flow across sites affect coevolutionary dynamics is beyond the scope of the present paper. However, it is possible to make informed hypotheses to this extent based on our results for the simpler case where gene flow is constant across all sites in a given network. To illustrate this, we focus on a spatial configuration that combines

two configurations, a star and a cycle (fig. D1). Because of this, it is likely that the dynamics of the whole network are driven by the collective dynamics of the star and the cycle.

To test this hypothesis, it is useful to note that the weighted adjacency matrix of the observed network can be written as the sum of two adjacency matrices: $A_{weighted} = A_{star} + A_{cycle}$. If we assume that gene flow magnitude is different in both sub-networks, we can write: $A_{weighted} = \alpha A_{star} + \beta A_{cycle}$. By varying α and β from 1 to 0, we get a scenario where gene flow is not constant across all sites. Thus, it is possible to assess whether our results would also hold in the case where gene flow is not constant across sites, and whether whole network dynamics can be understood as the collective dynamics of smaller, building sub-networks.

We find that the smaller the gene flow within any of the sub-networks, the less similar the dynamics become to what would be expected for the sub-network alone (fig. D2). For example, the smaller β is, the less similar is the dynamics to the cycle sub-network and the more similar the dynamics of the whole network are to the dynamics in the star sub-network. This suggests that some of our conclusions may hold in considerably more complex scenarios as far as it is possible to break down the observed structure into smaller sub-networks. However, we have also found some degree of non-linearity (fig. D2), suggesting that some combinations of spatial configurations might lead to idiosyncratic effects on coevolutionary dynamics.

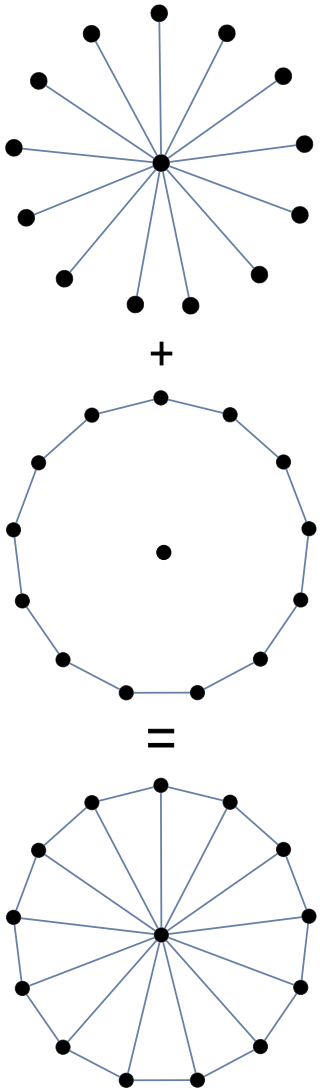

Figure D1: Depicts how the "observed" spatial network can be obtained by combining two sub-networks: a star, and a cycle.

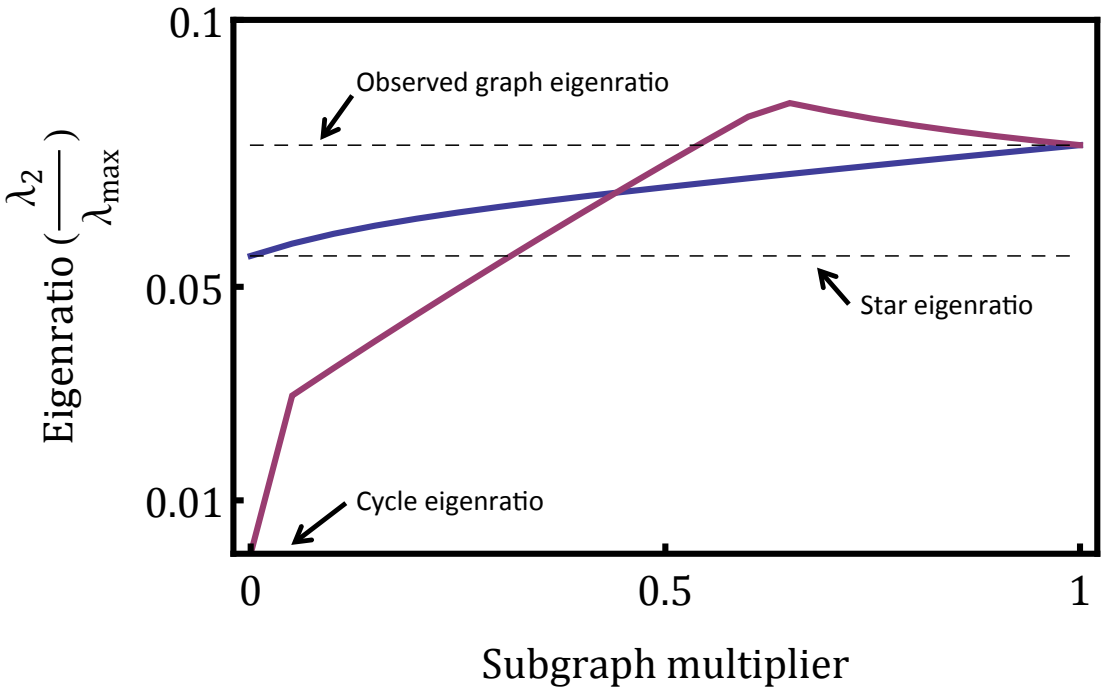

Figure D2: Plot of the eigenratio against the subgraph multiplier α (star multiplier, in red) and β (cycle multipler, in blue). The baseline values are $\alpha = \beta = 1$. For $\alpha = 0$ the eigenratio is zero, since there is one isolated site from the cycle and as a consequence the second smallest eigenvalue is also zero. As α goes from 0 to 1, the eigenratio shifts from zero to the eigenratio of the observed network. Also, as β goes from 0 to 1, the eigenratio goes from a star-like eigenratio to the eigenratio of the whole network. This suggests that the eigenratio of the entire network can indeed be understood as the collective dynamics of known sub-networks, even when gene flow is not constant across all sites.

E) Exploration of the space of parameters.

i) Baseline parameters:

Here we show the expected coevolutionary dynamics for specific combinations of gene flow strength (σ^2) and the strength of reciprocal selection (α). Because of the large space of parameters studied, we chose to show some particular combinations of σ^2 and α to give a better idea of the general dynamics expected for each structure. Here, σ^2 takes the values 0.19, 0.21, 0.25 and 0.31. Although these values look close to each other, the coevolutionary dynamics are very sensitive to a change in σ^2, allowing us to explore different qualitative dynamics both within and among spatial structures. In the case of α, we rather preferred to explore almost three orders of magnitude (0.002, 0.006, 0.01, and 0.1.), since coevolutionary dynamics are less sensitive to a change in the strength of reciprocal selection.

ii) Explanation of figures below:

Each of the pages below corresponds to the coevolutionary dynamics obtained for a single value of σ^2, and all possible α values. That is, there are four pages for each spatial structure, one for each of the σ^2 considered. Each of these pages has in turn four plots, corresponding to the four possible values of α. Also, each page is divided in four sections. The upper left section shows the spatial structure of considered. The upper right section, "α", indicates that below are plotted the coevolutionary dynamics for each value of α. The lower left section shows the value of σ^2 that is being considered in that page. Finally, the lower right section has four quadrants with a plot in each one, i.e. all possible coevolutionary dynamics for that given spatial structure and combination of gene flow strength and strength of reciprocal selection.

For each plot, the x-axis corresponds to time in generations ($\times 10^4$) and the y-axis corresponds to allelic frequency. The red curve tracks the change of one of the alleles of the parasitic species in the hotspot, while the blue curve tracks the change of one of the alleles of

the parasitic species in the closer coldspot to the considered hotspot (the allelic dynamics of the other species match the one considered but is slightly shifted). In the upper left corner, the spatial network depicted follows the same color code, indicating which coldspots and hotspots are being considered. We just plotted the coevolutionary dynamics of the parasitic species in order to simplify the visualization, since host and parasite dynamics are qualitatively the same (fig. A).

REFERENCES

Barahona, M. and L.M. Pecora. 2002. Synchronization in small-world systems. *Physical Review Letters* 89: 054101.

Cockerham, C. C., and B. S. Weir. 1993. Estimation of Gene Flow from F-Statistics. *Evolution* 47: 855–863.

Gomulkiewicz, R., J. N. Thompson, R. D. Holt, S. Nuismer and M. E. Hochberg. 2000. Hot spots, Cold spots, and the geographic mosaic theory of coevolution. *The American Naturalist* 156: 156-174.

———, S. Nuismer and J. N. Thompson. 2003. Coevolution in variable mutualisms. *The American Naturalist* 162: S80-S93.

Hofbauer, J. and K. Sigmund. 1998. Evolutionary Games and Population Dynamics. *Cambridge University Press*, Cambridge.

Holsinger, K. E., and B. S. Weir. 2009. Genetics in geographically structured populations: defining, estimating and interpreting F_{ST}. *Nature reviews, Genetics* 10: 639-650.

Koenig, W. D. and J. M. H. Knops. 1998. Scale of mast-seeding and tree-ring growth. *Nature* 396: 225-226.

Mohar, B. 1997. Some applications of Laplace eigenvalues of graphs. In *Graph Symmetry: Algebraic Methods and Applications*, G. Hahn and G. Sabidussi, eds., vol. 497 of NATO ASI Series C, Kluwer, pp. 227–275.

Nishikawa, T. and A.E. Motter. 2006. Synchronization is Optimal in non-diagonalizable networks. *Physical Review E* 73: 065106.

Nuismer, S., J. N. Thompson and R. Gomulkiewicz. 1999. Gene flow and geographically structured coevolution. *Proceedings of the Royal Society B* 266: 605-609.

Ohtsuki, H. and M.A. Nowak. 2006. The replicator equation on graphs. *Journal of Theoretical Biology* 243: 86-97.

Seger, J. 1988. Dynamics of some simple host-parasite models with more than two genotypes in each species. *Philosophical Transactions of the Royal Society B* 319:541-555.

Teschl, G. 2012. Ordinary Differential Equations and Dynamic Systems. *American Mathematical Society*. 353pp.

Thompson, J.N. 2005. The geographic mosaic of coevolution. *The University of Chicago Press.*